1   "Title"

2   Enhancement of zinc ion removal from water by physically-mixed particles of iron/iron sulfide

3

4

5   "Author name"

6   Yuya Kamba [1], Miharu Ueta [1], Md. Azhar Uddin [1], Yoshiei Kato [*1]

7

8   "Author address"

9   1: Department of Material and Energy Science, Graduate School of Environmental and Life Science,

10   Okayama University, 1-1 Tsushima-naka, 3-chome, Kita-ku, Okayama 700-8530 Japan

11

12   "Corresponding author"

13   *Yoshiei Kato, E-mail address: y-kato@cc.okayama-u.ac.jp

14

15

16

17 Abstract

18   Zinc (Zn) removal by physically-mixed particles of zero-valent iron (Fe) and iron sulfide (FeS) was

19   investigated as one technology for Zn removal from waste groundwater. The effects of the Fe/FeS mass

20   ratio, including a single Fe and FeS particles, and pH on changes in the concentrations of Zn, Fe and S were

21   examined by a batch test and column tests, and the mechanism of Zn elimination was discussed. Among all

22   the mixing fractions of Fe and FeS, Zn was eliminated most effectively by 3Fe/7FeS (mass ratio of Fe/FeS

23   =3/7). The Zn removal rate decreased in the order of 3Fe/7FeS, FeS and Fe, whereas the Fe concentration

24   decreased in the order of Fe, FeS and 3Fe/7FeS. The S concentration of FeS was larger than that of 3Fe/7FeS.

25   The Zn removal rate by physically-mixed 3Fe/7FeS particles was enhanced by a local cell reaction between

26   the Fe and FeS particles. The electrons caused by Fe corrosion moved to the FeS surface and reduced the

27   dissolved oxygen in the solution. Zn^{2+}, Fe^{2+} and OH^- ions in the solution were then coprecipitated on the

28   particles as $ZnFe_2(OH)_6$ and oxidized to $ZnFe_2O_4$. Moreover, Zn^{2+} was sulfurized as ZnS by both the Fe/FeS

29   mixture and the simple FeS particles. The Zn removal rate increased with increasing pH in the range from

30   pH 3 to 7. From a kinetic analysis of Zn removal, the rate constant of anode (Fe)/cathode (FeS) reaction

31   was almost the same as that of ZnS formation, and slightly larger than that of Fe alone.

32

33   Key words: Zero-valent iron, iron sulfide, zinc ion, zinc removal, groundwater treatment

34

1. Introduction

Many heavy metals in groundwater have a harmful impact on human health and the ecosystem due to their persistent toxicity. Although industrial plants are obliged to release effluents with heavy metal concentrations below effluent standards, contaminated water is occasionally released into groundwater when elimination and effluent monitoring of heavy metals are inadequate (Arao et al. 2010). Therefore, it is important to remediate groundwater contaminated by heavy metals (Hashim et al. 2011; Adeli et al. 2017; Dan'azumi and Bichi 2010; Inglezakis et al. 2003; Momodu and Anyakora 2010).

Zinc (Zn) metal is used in manufacturing hot-dip and electrogalvanized products, die-cast alloys, copper alloy products and so on, and was increasingly produced from a half century ago. Groundwater and soil have been contaminated by Zn-containing water discharged from industrial plants and mines (Kishimoto et al. 2018; Bhattacharya et al. 2006), which has been recognized as a serious environmental issue. Waste water from the plants of hot-dip and electrogalvanized products is especially contaminated by Zn alone (Ministry of the Environment, Government of Japan 2006). Zn is considered to be relatively nontoxic for human health (Fosmire 1990), but is toxic to fish and aqueous insects and plants (Iwasaki et al. 2009). In 2006, the Zn emission standard in Japan was decreased from 5 mg/L to 2 mg/L (Ministry of the Environment, Government of Japan 2006).

Various technologies for Zn removal from waste groundwater are available, including coagulation-flocculation (Kurniawan et al. 2006), ion exchange (Kurniawan 2006), adsorption (Kwon et al. 2005; Lu et al. 2007), ultrafiltration (Katsou et al. 2011) and electrodialysis (Kirkelund et al. 2010). Among these

54 treatment technologies, coagulating sedimentation is the most widely-used due to its simple equipment and

55 operation. As a drawback of this technology, because amphoteric Zn has a narrow pH range of 9 to 10.5 for

56 coagulation as zinc hydroxide, there is a danger of discharges exceeding the Zn effluent standard if

57 operational conditions unintentionally deviate from this range (Inamoto 2006).

58 Zero-valent iron has been also applied to groundwater remediation (Stokes and Moller 1999; Dries

59 et al. 2005; Rangsivek and Jekel 2005; Oh et al. 2007; Cundy et al. 2008; Kishimoto et al. 2011; Fu et al.

60 2014; Tosco et al. 2014; Lefevre et al. 2016; Kishimoto et al. 2018). Target heavy metals such as aluminum

61 (Al), cadmium (Cd), nickel (Ni) and Zn are precipitated by using the difference in their ionization

62 tendencies from Fe acting as a reductant, or are removed by iron coprecipitation and physical/chemical

63 adsorption on the iron surface (Kishimoto et al. 2018; Nobactep 2010). As the Zn removal mechanism in

64 water, Kishimoto et al. 2011 proposed that zero-valent iron is oxidized into ferric ion by dissolved oxygen,

65 iron hydroxide is then precipitated on the iron surface by the ferric ion, and finally the Zn ion is absorbed

66 on and/or coprecipitated with the ferric ion hydroxide.

67 Nakamaru et al. (2002; 2006) and Ono et al. (2005) found that a higher sulfur content in iron powder

68 promoted trichloroethylene (TCE) degradation in water and soil because local electrodes were formed

69 between iron (Fe: anode) and iron sulfide (FeS: cathode) partly precipitated on the Fe particle surface, and

70 reduction of TCE was enhanced on the FeS cathode. Instead of the high-S content iron described above,

71 FeS or iron disulfide (FeS_2) particles were physically mixed with Fe particles to materialize a local cell

4

72   reaction between the Fe and FeS particles, which are in mutual contact, and an increase in TCE degradation

73   in water was confirmed by a batch test (Shiba et al. 2014) and column tests (Demiya et al. 2018). TCE

74   degradation with originally synthesized Fe/FeS nanoparticles was also investigated by Kim et al. (2011;

75   2013; 2014). In research on removal of heavy metals from contaminated water, removal of arsenic (Min et

76   al. 2017), cadmium (Su et al. 2015) and chromium (Gong et al. 2017) was accelerated by the high reactivity

77   of S with the metal and the chemical stability of the formed metallic sulfide. However, little research has

78   been done on Zn removal by Fe/FeS mixed particles. Therefore, in the present study, the effects of the

79   Fe/FeS mass ratio and pH on the change in the Zn^{2+} concentration in water were investigated to obtain an

80   optimal Fe/FeS composition, and a Zn elimination mechanism was proposed based on batch and column

81   tests. Contribution of Fe-FeS, Fe and FeS to a Zn removal rate was calculated by a kinetic model.

82

83

84   2. Experimental

85   2.1 Sample preparation

86   100 mg/L Zn solution was prepared by using $Zn(NO_3)_2 \cdot 6H_2O$. Putting together 0.1 M HNO_3 or 0.1

87   M NaOH, the pH values in the solution were varied to 3, 5.6 and 7. Fe (255MC, JFE steel) and FeS

88   (FUJIFILM Wako Pure Chemical) were used for the experiments. The mean diameter of Fe particles was

89   185 μm, whereas FeS was pulverized between 140 and 200 μm by a grinding mill (Wonder Blender,

90   OSAKA CHEMICAL). The density, ρ_i, and specific surface area, γ_i, of i (=Fe, FeS) are shown in Table 1.

91   γ_{FeS} (= 0.30 m^2/g) value was larger than γ_{Fe} (= 0.17 m^2/g). The samples used for the experiments were

92   composed of Fe, FeS, Fe/FeS (mixture of Fe and FeS) particles. The Fe/FeS particles sample was

93   premixed for 10 h by a rotator (VMRG-5, AS ONE) to obtain a homogeneous mixture. The experimental

94   temperature was about 298 K.

95

96   2.2 Experimental procedure

97   2.2.1 Batch test

98   A 2.3 g sample and 100 mg/L Zn solution were added to a 30 mL vial bottle without headspace and

99   mixed with a rotator (VMRG-5, AS ONE) at a rotation speed of 100 rpm for 3 h. The Fe, FeS and Fe/FeS

100   (mass ratio: 7/3, 5/5, 3/7, 1/9) samples were tested at a constant temperature of 298 K. The supernatant

101   solution after filtration was diluted with a 0.1 M HNO$_3$ solution, and the Zn, Fe and S ion concentrations

102   were measured by inductively coupled plasma atomic emission spectrometry (ICP-AES) (Visa-PRO,

103   Seiko Instruments).

104   2.2.2 Column tests

105   Figure 1 shows a schematic diagram of the column-type experimental apparatus. A 10 g sample was

106   packed in a glass column (inner diameter: 13.5 mm, height: 360 mm). The Fe, FeS and Fe/FeS (mass

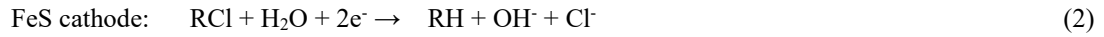107   ratio: 3/7) samples were used in the experiments. A 100 mg/L Zn solution was supplied inside the column

108 upward at a flow rate of 2.0 mL/min. The solution temperature was kept at 298 K by flowing tap water

109 throughout the outer cylinder of the column. The starting time, t, of the experiment was defined as 0 when

110 the solution began to reach the sampling site. The 0.2 mL treated solution was withdrawn at 10, 20, 30,

111 40, 50, 60, 90, 120 and 180 min and diluted with 0.1 M HNO_3, and the Zn, Fe and S ion concentrations

112 were measured by the ICP-AES, as in the batch test. The dried sample after treatment was analyzed with

113 an X-Ray diffractometer (XRD) (RINT-2100, Rigaku).

114

115 3. Results and discussion

116 3.1 Effect of mass ratio of Fe/FeS on Zn removal rate

117 　　　The batch test was carried out to clarify the effect of the mass ratio of Fe to FeS on Zn removal and

118 Fe dissolution in the solution, as shown in Fig. 2. The pH value was kept at 5.6 with no addition of 0.1 M

119 HNO_3 or 0.1 M NaOH. The lowest Zn concentration was obtained at the mass ratio of Fe/FeS = 3/7

120 (3Fe/7FeS), and the lowest Fe concentration also occurred at around Fe/FeS of 3/7. Therefore, the

121 mixture of Fe and FeS particles was studied under the 3Fe/7FeS condition. Shiba et al. (2014) indicated

122 that the TCE degradation rate was highest under the 3Fe/7FeS condition, while the γ_{Fe} and γ_{FeS} values

123 were 0.17 and 0.34 m^2/g, respectively, because the local cell reaction between Fe (anode) and FeS

124 (cathode) proceeded most efficiently in this condition, as follows:

125 　　　Fe anode: 　　　　$Fe \rightarrow Fe^{2+} + 2e^-$ 　　　　　　　　　　　　　　　　　　　　　(1)

126   FeS cathode: $RCl + H_2O + 2e^- \rightarrow \quad RH + OH^- + Cl^-$ (2)

127   Here, RCl is TCE (trichloroethylene: $ClCH=CCl_2$).

128   The specific surface areas of Fe (= 0.16 m^2/g) and FeS (=0.30 m^2/g,) in the present study were also

129   similar to the TCE degradation condition in the above-mentioned study, suggesting that the Zn removal

130   rate was also promoted most effectively.

131

132   3.2 Effect of pH on Zn removal rate for Fe, 3Fe/7FeS and FeS

133   The temporal changes in the Zn removal rate and Fe and S concentrations in the column tests with

134   the Fe, 3Fe/7FeS and FeS samples were compared. The graphs for the tests with pH = 3, 5.6 and 7 are

135   shown in Figs. 3, 4 and 5, respectively. Here, the Zn removal rate, R (%), was defined as shown in Eq.

136   (3).

137    $$R = \frac{C_0 - C(t)}{C_0} \times 100$$ (3)

138   where, R is the Zn removal rate (%), C_0 is the initial Zn^{2+} concentration (mg/L) and $C(t)$ is the Zn^{2+}

139   concentration (mg/L) at time, t (h).

140   The Zn removal rate and Fe and S concentrations of all samples gradually decreased with time.

141   This suggests that the surface area for Zn removal and the number of Fe and S dissolution sites decreased.

142   The Zn removal rate decreased in the order of 3Fe/7FeS, FeS and Fe, whereas the Fe concentration

143   decreased in the order of Fe, FeS and 3Fe/7FeS. In addition, the S concentration of FeS was larger than

144   that of 3Fe/7FeS. The above tendencies applied to all figures of Figs. 3 to 5. The enhancement of the Zn

145   removal rate resulted in higher consumption of Fe and S dissolved in the solution, and thereby caused the

146   decrease in the Fe and S concentrations.

147   In all samples, the pH increase enhanced the Zn removal rate, as also reported by Kishimoto et al.

148   (2011) and Rangsivek and Jekel (2005), and decreased the Fe and S concentrations. At pH = 7, the Zn

149   removal rate of 3Fe/7FeS was maintained at almost 100 %, and even the simple Fe sample eliminated

150   more than 80 % of the Zn^{2+} in the solution in this study. The enhancement of the Zn removal rate by the

151   larger pH value is estimated to be due to Zn^{2+} precipitation, as discussed in the following section.

152

153   3.3 Mechanism of Zn removal

154   XRD analyses of the samples were carried out before/after the experiment. The XRD patterns of

155   3Fe/7FeS and FeS, and Fe at pH = 5.6 are shown in Fig. 6 (A) and Fig. 6 (B), respectively. $ZnFe_2O_4$, Fe,

156   FeS and ZnS were detected after the treatment. Interestingly, Fe was found even in the FeS sample.

157   Firstly, it is suggested that the $ZnFe_2O_4$ was formed by the following coprecipitation (Eq. (4)) (Tokumura

158   and Kawase, 2013) and sequential oxidation reactions of $ZnFe_2(OH)_6$ (Eq. (5)).

159        $$Zn^{2+} + 2Fe^{2+} + 6OH^- \rightarrow ZnFe_2(OH)_6 \tag{4}$$

160        $$ZnFe_2(OH)_6 + 1/2O_2 \rightarrow ZnFe_2O_4 + 3H_2O \tag{5}$$

161   Here, O_2 of Eq. (5) depends on the dissolved oxygen under an aerobic condition of the solution or the

162 sample drying procedure before the XRD measurement. Eq. (4) indicates that a larger OH⁻ (higher pH

163 value) promotes $ZnFe_2(OH)_6$ formation thermodynamically, which causes the enhancement of the Zn

164 removal rate seen in Section 3.2.

165   The detected ZnS resulted from the following reaction (Eq. (6)), which indicates higher Zn removal

166 rates by the 3Fe/7FeS and FeS samples.

167     $Zn^{2+} + S^{2-} \rightarrow ZnS$ (6)

168   The observed Fe in the FeS sample after the experiment is due to the S^{2-} dissolution reaction, as

169 follows:

170 $FeS + 2e^- \rightarrow Fe + S^{2-}$ (7)

171 The electrons in Eq. (7) were generated by Fe dissolution ($Fe \rightarrow Fe^{2+}$) and were transferred from the Fe

172 particles to the FeS particles.

173   The results of the XRD analyses of the samples at pH = 3 and 7 are shown in Fig. 7. Even under the

174 higher acidity (pH = 3) and neutral (pH = 7) conditions, $ZnFe_2O_4$ was detected in all samples, and ZnS

175 was detected in the 3FeS/7FeS and FeS samples after the treatment, as in Fig. 6. On the other hand, Fe

176 was detected in the Fe sample at pH = 3 and 5.6, but was not observed in the 3Fe/7FeS and FeS samples

177 at pH = 7 (neutrality). As shown in Figs. 3 to 5, the decreased S dissolution with increasing pH inhibited

178 the reaction of Eq. (7) and the Fe formation on the FeS.

179   Based on the above facts, the Zn removal sites of the Fe/FeS particles are as shown schematically

10

180   in Fig. 8. Both electrons and Fe^{2+} are more easily generated by a local cell reaction between particles of

181   Fe (anode) and FeS (cathode) (Shiba et al. 2014; Demiya et al. 2018). The electrons move from Fe to FeS

182   particles and reduce the dissolved oxygen (O_2) to the hydroxyl ion (OH^-) in addition to the S^{2-} dissolution

183   in Eq. (7). Zinc iron hydroxide ($ZnFe_2(OH)_6$) is then formed by the chemical coprecipitation of Zn^{2+}, Fe^{2+}

184   and OH^-, and subsequently, this compound is partially oxidized to zinc ferrite ($ZnFe_2O_4$), as indicated in

185   the right and left sides of Fig. 8. The formation of $ZnFe_2(OH)_6$ and $ZnFe_2O_4$ by simple Fe or FeS particles

186   was also observed in Figs. 6 and 7, although a larger number of unreacted zinc ions remained in the

187   solution in comparison with the Fe/FeS particles, as shown in Figs. 2 to 5. This is thought to be due to an

188   incomplete local cell reaction. The above process is described by the following reactions:

189   Anode reaction (iron corrosion):

190          $Fe \rightarrow Fe^{2+} + 2e^-$ (8)
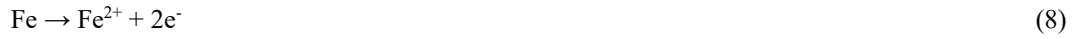
191   Cathode reaction (reduction of dissolved oxygen):

192          $O_2 + 2H_2O + 4e^- \rightarrow 4OH^-$ (9)

193   Coprecipitation of Zn^{2+} and Fe^{2+}:

194          $Zn^{2+} + 2Fe^{2+} + 6OH^- \rightarrow ZnFe_2(OH)_6$ (4)

195   Oxidation of zinc-iron hydroxide (reduction of dissolved oxygen):

196          $ZnFe_2(OH)_6 + 1/2O_2 \rightarrow ZnFe_2O_4 + 3H_2O$ (5)

197   Zn^{2+} was sulfurized by S^{2-} as follows:

198   Sulfurization:

199        $Zn^{2+} + S^{2-} \rightarrow ZnS$ (6)
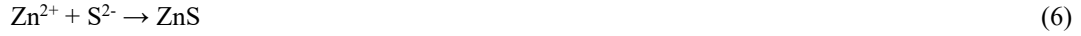
200   In this study, because the physically-mixed particles of 3Fe/7FeS (optimal combination of Fe and

201   FeS) displayed more efficient Zn removal than Fe and FeS in all cases, the local cell reaction between Fe

202   and FeS was the key factor for enhancement of the Zn removal rate. XPS (X-ray Photoelectron

203   Spectrometry) is effective to analyze an elementary composition and chemical-bonding state just below

204   some nanometers from a sample surface. As the next logical step, these results obtained from the XRD

205   measurement must be confirmed by the XPS analysis.

206

207   3.4 Kinetic model of Zn removal rate

208   In this section, a kinetic model of Zn removal is indicated by using the results of batch test. The Zn

209   removal occurred by the coprecipitation in Eq. (4) and sulfurization in Eq. (6) as seen in Fig. 8. From the

210   batch test in Fig. 2, the most rapid Zn removal rate was obtained at Fe/FeS of 3/7 due to the most efficient

211   Fe (anode) – FeS (cathode) coprecipitation reaction in addition to the Zn sulfurization. Thus, supposing

212   that the Zn removal occurred at FeS surface in the whole range of Fe/FeS and additionally at Fe surface

213   for Fe/FeS > 3/7 as well as Shiba et al. (2014) and Demiya et al. (2018), and the Zn removal rate was

214   proportional to the Zn concentration, the following equations were given,

215        $-\dfrac{dC(t)}{dt} = KC(t)$ (7)

12

216 $$K = k_{\text{Fe-FeS}} a_{\text{FeS}} + k_{\text{FeS}} a_{\text{FeS}} + k_{\text{Fe}} a_{\text{Fe}} \qquad (8)$$

217 where, K is the overall rate constant (h^{-1}), $k_{\text{Fe-FeS}}$, k_{FeS} and k_{Fe} are the rate constants (m/h) of Zn removal by

218 anode-cathode reaction between Fe and FeS (coprecipitation), ZnS formation due to FeS dissolution

219 (sulfurization), and additional anode-cathode reaction at Fe surface (coprecipitation), respectively, a_{FeS}

220 and a_{Fe} are the effective surface area (m^2) of FeS and Fe particles, respectively.

221   At Fe/FeS < 3/7, a_{Fe} became 0, and Eq. (7) and a_{FeS} are expressed by Eqs. (9) and (10), respectively.

222 $$-\frac{\mathrm{d}C(t)}{\mathrm{d}t} = (k_{\text{Fe-FeS}} a_{\text{FeS}} + k_{\text{FeS}} a_{\text{FeS}})\, C(t) \qquad (9)$$

223 $$a_{\text{FeS}} = W_{\text{FeS}}\, \gamma_{\text{FeS}} / V \qquad (10)$$

224 where, W_{FeS} is the mass (g) of FeS and V is the Zn solution volume (m^3).

225   At Fe/FeS > 3/7, the anode-cathode reaction occurs in Fe particle alone in addition to Fe-FeS, and

226 the effective surface area, a_{Fe}, of Fe is given by the following equation.

227 $$a_{\text{Fe}} = W'_{\text{Fe}}\, \gamma_{\text{Fe}} / V \qquad (11)$$

228 $$W'_{\text{Fe}} = W_{\text{Fe}} - [(\text{mass\% Fe})/(\text{mass\% FeS})]_{\text{peak}}\, W_{\text{FeS}} \qquad (12)$$

229 where, W'_{Fe} is the mass (g) of Fe without contribution of the Fe (anode) – FeS (cathode) reaction,

230 $[(\text{mass\% Fe})/(\text{mass\% FeS})]_{\text{peak}}$ is the mass ratio of Fe/FeS to obtain the maximum Zn removal rate (=3/7).

231   By substituting $a_{\text{FeS}} = 0$ in Eq. (8) and $W_{\text{FeS}} = 0$ in Eq. (12) for the Fe particles alone, and $k_{\text{Fe-FeS}} = 0$ in

232 Eq. (9) for FeS particles alone, $k_{\text{Fe}} = 8.77 \times 10^{-6}$ m/h and $k_{\text{FeS}} = 1.26 \times 10^{-5}$ m/h were obtained from the batch

233 test data, respectively. The $k_{\text{Fe-FeS}}$ values were calculated from Eqs. (9)-(12) by using these k_{Fe} and k_{FeS}.

234   The relationship between k_{Fe-FeS} and mass ratio of Fe/FeS is shown in Fig. 9. The average k_{Fe-FeS} value of

235   Fe/FeS=7/3, 5/5 and 3/7 became 1.25×10^{-5} m/h. Compared between k_{Fe}, k_{Fe-FeS} and k_{FeS} values, the anode-

236   cathode reaction rate between Fe and FeS particles was almost same as the sulfurization of FeS, and

237   slightly larger than the anode-cathode reaction rate within Fe particles. The magnitude of average k_{Fe-FeS}

238   ($=1.25 \times 10^{-5}$ m/h) for Zn removal in this study was 4.8 times as large as that for TCE dechlorination

239   (Demiya et al. 2018). The effects of the operation parameters such as Zn concentration, particle diameters

240   of Fe and FeS, respectively, and mass ratio of Fe/FeS on the Zn removal rate are predictable by using the

241   above rate constant values of the batch test.

242   These k_i (i=Fe-FeS, Fe, FeS) values were also applicable to the reaction rate of column tests,

243   however, the overall Zn removal rate decreases with time due to laminar flow with very slow velocity

244   which makes it difficult to peel the adsorbent such as $ZnFe_2O_4$ and ZnS on the FeS and Fe particles. The

245   Zn removal reaction model for the column test is needed to consider the peeling factors as well.

246

247   4. Conclusions

248   Zn removal from a solution by Fe, Fe/FeS and FeS particles was investigated in batch and column

249   tests. Compared with simple Fe or FeS particles, the Zn removal rate by physically-mixed particles of

250   3Fe/7FeS (mass ratio of Fe/FeS =3/7) was enhanced due to a local cell reaction between the Fe and FeS.

251   The electrons caused by Fe corrosion moved to the FeS surface and reduced the dissolved oxygen in the

14

252   solution. Zn^{2+}, Fe^{2+} and OH^- ions in the solution were then coprecipitated on the particle surface as

253     $ZnFe_2(OH)_6$ and oxidized to $ZnFe_2O_4$. Moreover, Zn^{2+} was sulfurized as ZnS by both the FeS of the

254   Fe/FeS mixture and the simple FeS particles. In this study, the Zn removal rate increased with increasing

255   pH in the range of pH 3 to 7.

256

257

258   References

259   Adeli, M., Yamini, Y., Faraji, M., (2017). Removal of copper, nickel and zinc by sodium dodecyl sulphate

260   coated magnetite nanoparticles from water and wastewater samples, *Arabian Journal of Chemistry*,

261   10, S514-S521.

262   Arao, T., Ishikawa S., Murakami M., Abe K., Maejima Y., Makino T., (2010). Heavy metal contamination

263   of agricultural soil and countermeasures in Japan. *Paddy and Water Environment*, 8, 247-257.

264   Bhattacharya, A.K., Mandal, S.N., Das, S.K., (2006). Adsorption of Zn(II) from aqueous solution by using

265   different adsorbents. *Chemical Engineering Journal*, 123, 43–51(2006).

266   Cundy, A. B., Hopkinson, L., Whitby, R. L. D., (2008). Use of iron-based technologies in contaminated

267   land and groundwater remediation: a review. *Science of The Total Environment*, 400, 42-51.

268   Dan'azumi, S., Bichi, M. H., (2010). Industrial pollution and heavy metals profile of Challawa river in

269   Kano, Nigeria. *Journal of Applied Sciences and Environmental Sanitation*, 5, 56-62.

270   Demiya, M., Uddin, M. A., Kato, Y., (2018). Enhancement in trichloroethylene dechlorination by mixed

271   particles of iron-iron disulfide or iron-iron sulfide. *Journal of Environmental Chemical Engineering*,

272   6, 1020-1026.

273   Dries, J., Bastiaens, L., Springael D., Kuypers, S., Agathos S. P., Diels, L., (2005). Effect of humic acids

274   on heavy metal removal by zero-valent iron in batch and continuous flow column systems. *Water*

275   *Research*, 39, 3531-3540.

276   Fosmire, G.J., (1990). Zinc toxicity, *The American Journal of Clinical Nutrition*, 51, 225–227.

277   Fu, F., Dionysiou, D. D., Liu H., (2014). The use of zero-valent iron for groundwater remediation and

278   wastewater treatment: a review. *Journal of Hazardous Materials,* 267, 1994-205.

279   Gong, Y., Gai, L., Tang, J., Fu, J., Wang, Q., Zeng, E. Y., (2017). Reduction of Cr(VI) in simulated g

280   groundwater by FeS-coated iron magnetic nanoparticles. *Science of the Total Environment*, 595, 743-

281   751.

282   Hashim, M. A., Mukhopadhyay, S., Sahu, J. N., Sengupta, B., (2011). Remediation technologies for heavy

283   metal contaminated groundwater. *Journal of Environmental Management*, 92, 2355-2388.

284   Inamoto, J., (2006). Waste water treatment for plating. *Journal of the Surface Finishing Society of Japan*,

285   57, 889-894

286   Inglezakis, V. J., Loizidou, M. D., Grigoropoulou H. P., (2003). Ion exchange of Pb^{2+}, Cu^{2+}, Fe^{3+}, and Cr^{3+}

287   on natural clinoptilolite: selectivity determination and influence of acidity on metal uptake. *Journal*

288   *of Colloid Science*, 261, 49-54.

289   Iwasaki, Y., Kagaya, T., Miyamoto, K., Matsuda, H., (2009). Effects of heavy metals on riverine benthic

290   macroinvertebrate assemblages with reference to potential food availability for drift-feeding fishes,

291   *Environmental Toxicology and Chemistry*, 28, 354–363.

292   Katsou, E., Malamis, S., Haralambous, K. J., (2011). Industrial wastewater pre-treatment for heavy metal

293   reduction by employing a sorbent-assisted ultrafiltration system. Chemosphere, 82, 557-564.

294   Kim, E.-J., Kim, J.-H., Azad, A-M., Chang, Y.-S., (2011). Facile synthesis and characterization of Fe/FeS

295   nanoparticles for environmental applications. A*CS Applied Materials & Interfaces*, 3, 1457-1462.

296   Kim, E.-J., Kim, J.-H., Chang, Y.-S., Turcio-Ortega, D., Trantnyek, P.G., (2014). Effects of metal ions on

297   the reactivity and corrosion electrochemistry of Fe/FeS nanoparticles. *Environmental Science &*

298   *Technology*, 48, 4002-4011.

299   Kim, E.-J., Murugesan, K., Kim, J.-H., Tratnyek, P. G., Chang, Y.-S., (2013). Remediation of

300   trichloroethylene by FeS-coated iron nanoparticles in simulated and real groundwater: effects of

301   water chemistry. *Industrial & Engineering Chemistry Research*, 52, 9343-9350.

302   Kirkelund, G. M., Ottosen, L. M., Villumsen, A., (2010). Investigation of Cu, Pb and Zn partitioning by

303   sequential extraction in harbor sediments after electrodialytic remediation. Chemosphere, 79, 997-

304   1002.

305   Kishimoto, N., Narazaki, Y., Takemoto, K., (2018). Reusability of zero-valent iron particles for zinc ion

306   separation. *Separation and Purification Technology*, 193, 139–146.

307   Kishimoto, N., Iwano S., Narazaki Y., (2011). Mechanistic consideration of zinc ion removal by zero-valent

308   iron. *Water, Air, and Soil Pollution*, 221, 183-189.

309   Kurniawan, T.A. , Chan, G.Y.S. , Lo, W.H. , Babel, S., (2006). Physico–chemical treatment techniques for

310   wastewater laden with heavy metals. *Chemical Engineering Journal*, 118, 83–98.

311   Kwon, J-S., Yun, S-T., Kim, S-O., Mayer B., Hutcheon I., (2005). Sorption of Zn(II) in aqueous solutions

312   by scoria. *Chemosphere*, 60, 1416-1426.

313   Lefevre, E., Bossa, N., Wiesner, M. R., Gunsch, C. K., (2016). A review of environmental implications of

314   *in situ* remediation by nanoscale zero valent iron (nZVI): behavior, transport and impacts on

315   microbial communities. *Science of The Total Environment*, 565, 889-901.

316   Lu, S., Gibb, S. W., Cochrane, E., (2007). Effective removal of zinc ions from aqueous solutions using crab

317   carapace biosorbent. *Journal of Hazardous Materials,* 149, 208-217.

318   Min, X., Li, Y., Ke, Y., Shi, M., Chai, L., Xue, K., (2017). Fe-FeS$_2$ adsorbent prepared with iron powder

319   and pyrite by facile ball milling and its application for arsenic removal. *Water Science & Technology*,

320   76, 192-200.

321   Ministry of the Environment, Government of Japan, (2006). https://www.env.go.jp/hourei/05/000001.html

322   Momodu, M.A., Anyakora, C.A., (2010), Heavy metal contamination of ground water: the surulere case

323   study. *Research Journal Environmental and Earth Sciences*, 2, 39-43.

324   Nakamaru, H., Ono, T., Kato, Y., Ogura, K., (2002). Effect of the microstructure of an iron powder on the

325   reactivity with trichloroethylene. *ACS Division of Environmental chemistry*, 42. 555-559.

326   Nakamaru, H., Ono, T., Kato, Y., Ogura, K., (2006). Properties of sulfur-contained iron powder suitable for

327   degradation of chlorinated organic compounds. *Nihon Kinzoku Gakkai Shi*, 70, 809-815.

328   Noubactep, C., (2010). Elemental metals for environmental remediation: learning from cementation process.

329   *Journal of Hazardous Materials,* 181, 1170-1174.

330   Oh, B.-T., Lee, J.-Y., Yoon, J., (2007). Removal of contaminants in leachate from landfill by waste steel

331   scrap and converter slag. *Environmental Geochemistry Health*, 29, 331-336.

332   Ono, T., Nakamaru, H., Kato, Y., Ogura K., (2005). Iron powder for remediation of contaminated soil, *JFE*

333   *Giho*, 7, 29-33.

334   Rangsivek, R., Jekel, M. R., (2005) Removal of dissolved metals by zero-valent iron (ZVI): Kinetics,

335   equilibria, processes and implications for stormwater runoff treatment. *Water Research*, 39, 4153-

336   4163.

337   Shokes, T. E., Moller, G., (1999) Removal of dissolved heavy metals from acid rock drainage using iron

338   metal. *Environmental Science and Technology*, 33, 282-287.

339   Shiba, M., Uddin, M. A., Kato, Y., Ono, T., (2014). Degradation of chlorinated organic compounds by

340   mixed particles of iron/iron sulfide or iron/disulfide. *Material Transactions*, 55, 708-712.

341   Su, Y., Adeleye, A. S., Keller, A. A., Huang, Y., Dai, C., Zhou, X., Zhang, Y., (2015). Magnetic sulfide-

342   modified nanoscale zerovalent iron (S-nZVI) for dissolved metal ion removal. *Water Research*, 74,

343   47-57.

344   Tokumura, M., Kawase, Y., (2013). Teppun (ZVI) wo motiita mizusyori gijyutu (Water treatment

345   technology by zero-valent iron (ZVI)). *Yosui-toHaisui*, 55, 574-581.

346   Tosco, T., Papini, M. P., Viggi, C. C., Sethi R., (2014). Nanoscale zerovalent iron particles for groundwater

347   remediation: a review. *Journal of Cleaner Production*, 77, 10-21.

348

349   Figures and Table captions

350

351   Fig. 1 Schematic diagram of column equipment

352   Fig. 2 Effect of Fe/FeS mass ratio on Zn and Fe concentrations (batch test, pH=5.6)

353   Fig. 3 Comparison of temporal change in Zn removal rate and Fe and S concentrations between iron-based

354   samples (column test, pH=3)

355   Fig. 4 Comparison of temporal change in Zn removal rate and Fe and S concentrations between iron-based

356   samples (column test, pH=5.6)

357   Fig. 5 Comparison of temporal change in Zn removal rate and Fe and S concentrations between iron-based

358   samples (column test, pH=7)

359   Fig. 6 X-ray diffraction patterns of 3Fe/7FeS, FeS and Fe samples before/after column test (pH=5.6).

360   Fig. 7 X-ray diffraction patterns of 3Fe/7FeS, FeS and Fe samples after column test (pH=3, 7).

361   Fig. 8 Schematic diagram of Zn removal sites of Fe/FeS particles.

362   Fig. 9 Relationship between rate constant of Zn removal by coprecipitation and mass ratio of Fe/FeS.

363

364   Table 1 Particle density and specific surface area of Fe and FeS

365

366

367

368

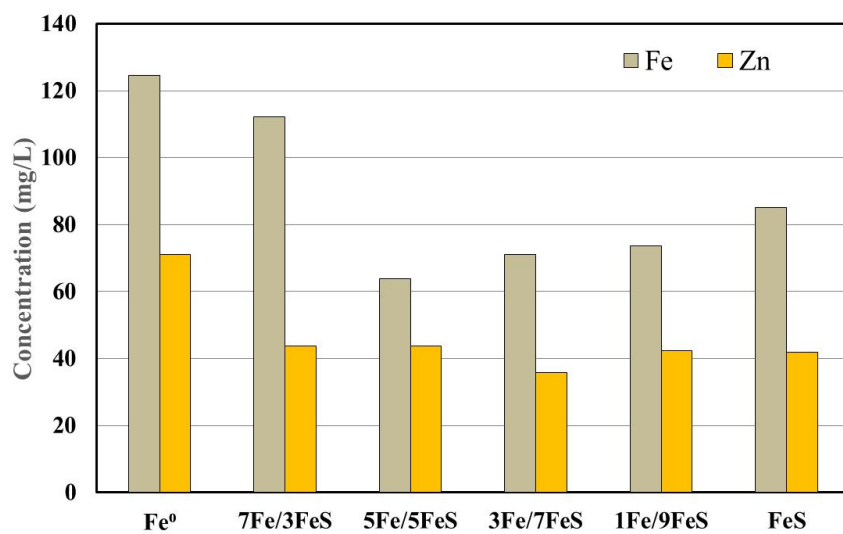369

370

371
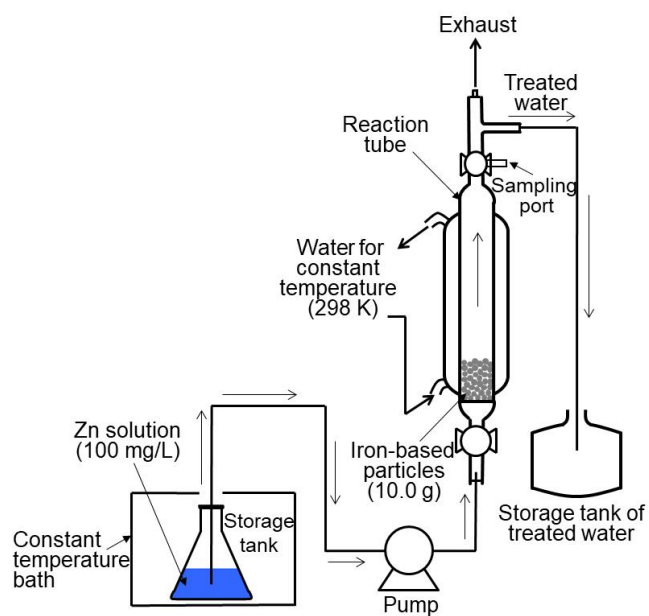
Fig. 1 Schematic diagram of column equipment

373

374

375

376

377

378

379   Fig. 2 Effect of Fe/FeS mass ratio on Zn and Fe concentrations (batch test, pH=5.6)
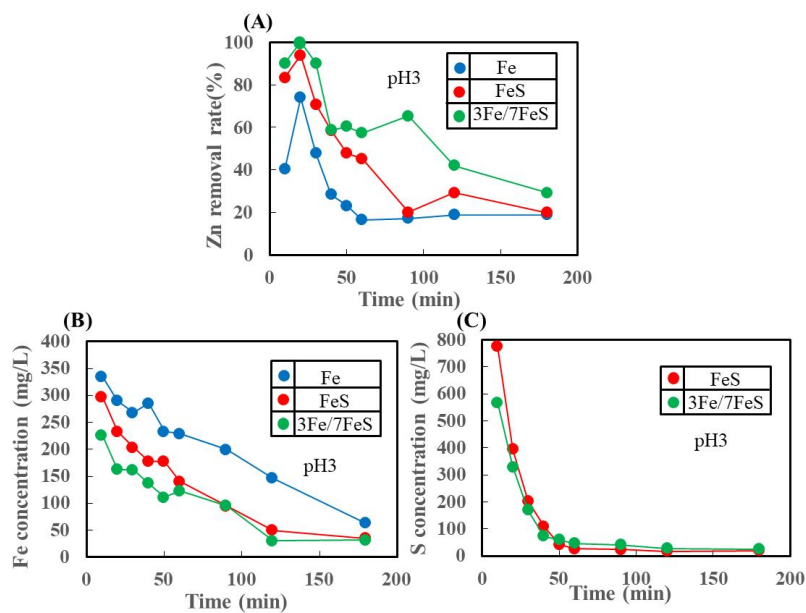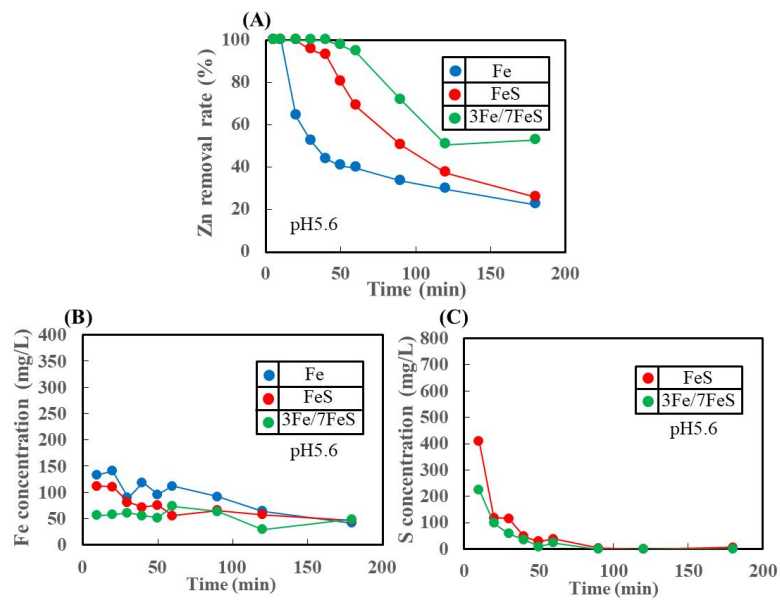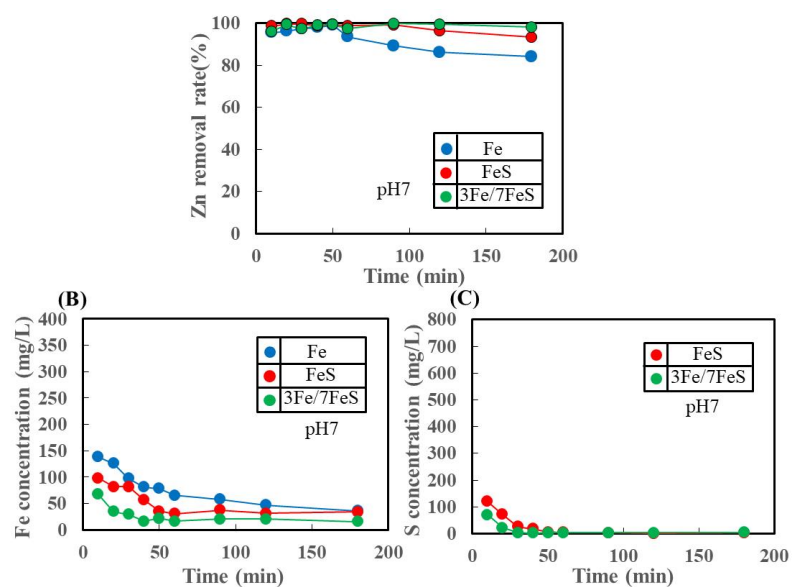
380

381

382

383

384

385

386

387

388 Fig. 3 Comparison of temporal change in Zn removal rate, and Fe and S concentrations
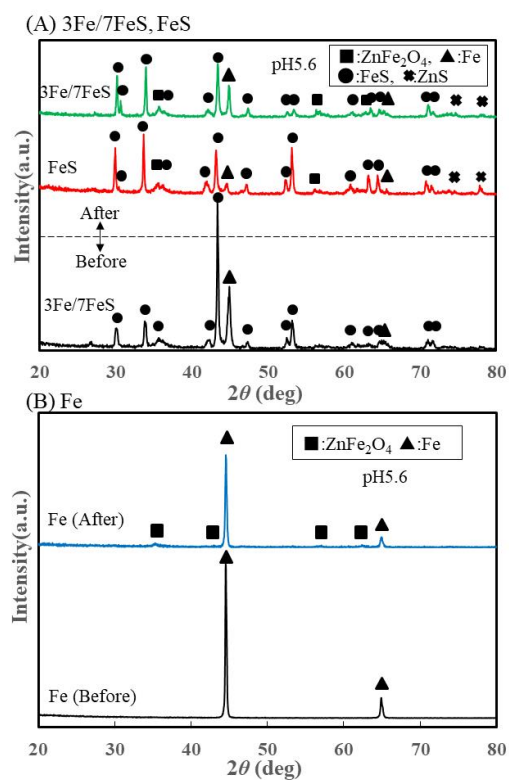
389 between iron-based samples (column test, pH=3)

390

391

392

393

394

395

396

397　Fig. 4 Comparison of temporal change in Zn removal rate, and Fe and S concentrations between iron-

398　based samples (column test, pH=5.6)

399

400

401

402

403

404

Fig. 5 Comparison of temporal change in Zn removal rate, and Fe and S concentrations between iron-

based samples (column test, pH=7)

407

408

409

410

(A) 3Fe/7FeS, FeS

(B) Fe

411

412

413   Fig. 6 X-ray diffraction patterns of 3Fe/7FeS, FeS and Fe samples before/after column test (pH=5.6).

414

415

416

417

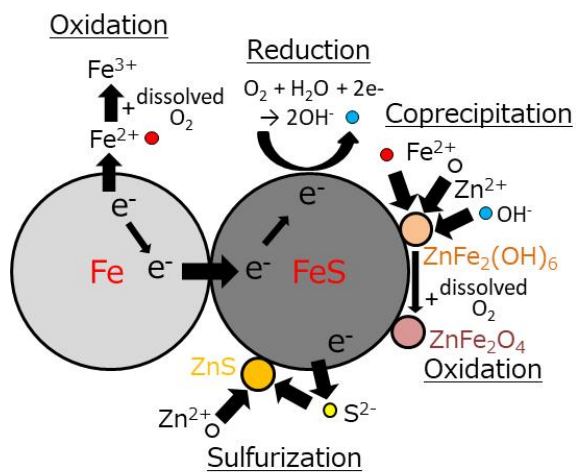Fig. 7 X-ray diffraction patterns of 3Fe/7FeS, FeS and Fe samples after column test (pH=3, 7).

420

421

422

423

424

425

426

Fig. 8 Schematic diagram of Zn removal sites of Fe/FeS particles.

427
428
429

430

431
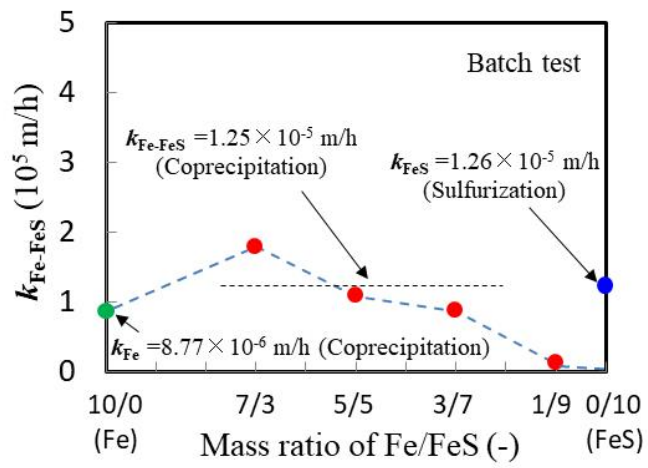

Fig. 9 Relationship between rate constant of Zn removal by coprecipitation and mass ratio of Fe/FeS.

432

433

434

436

437

438   Table 1 Particle density and specific surface area of Fe and FeS

439

	Density（kg/m³)	Specific surface area (m²/g)
Fe	7.87×10^3	0.160
FeS	4.85×10^3	0.304

440